Volume 11
Number 19
21 May 2023
Pages 4145–4368

# Journal of Materials Chemistry B

Materials for biology and medicine

rsc.li/materials-b

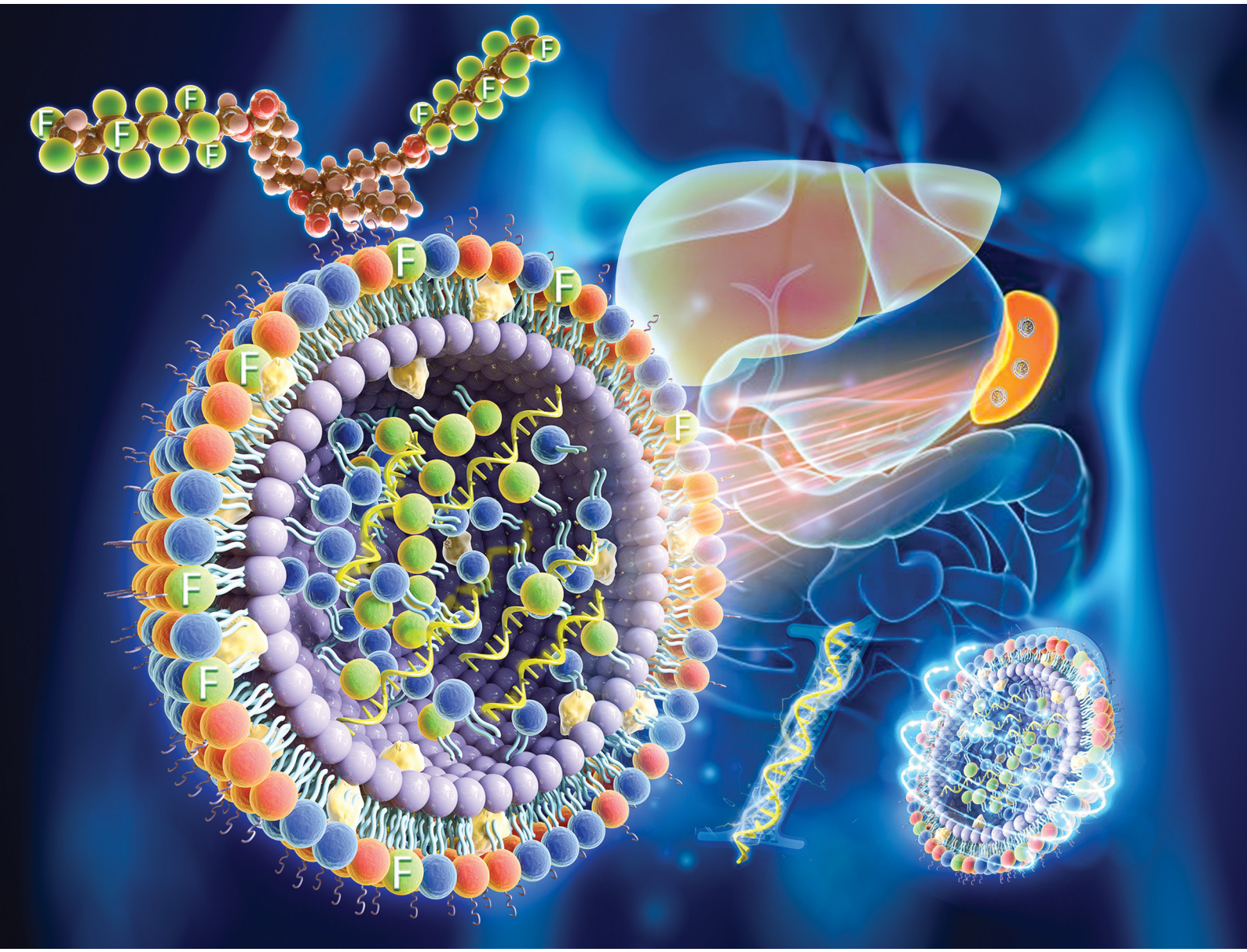


ISSN 2050-750X

ROYAL SOCIETY OF CHEMISTRY

**PAPER**

Jiaqi Lin, Ning Chen, Xueguang Lu *et al.*
A fluorinated ionizable lipid improves the mRNA delivery efficiency of lipid nanoparticles

10 YEARS ANNIVERSARY

Journal of Materials Chemistry B

ROYAL SOCIETY OF CHEMISTRY

PAPER

View Article Online
View Journal | View Issue



Cite this: J. Mater. Chem. B, 2023, 11, 4171

# A fluorinated ionizable lipid improves the mRNA delivery efficiency of lipid nanoparticles†

Haonan Huo,‡[ab] Xingdi Cheng,‡[a] Jiaxi Xu,[c] Jiaqi Lin,*[d] Ning Chen*[c] and Xueguang Lu*[ab]

Received 11th March 2023,
Accepted 11th April 2023

DOI: 10.1039/d3tb00516j

rsc.li/materials-b

The efficacy of messenger RNA (mRNA)-based vaccines or therapies relies on delivery vehicles that can transport them into the cytosol of cells. Lipid nanoparticles (LNPs) are the most clinically advanced carrier for mRNA. The chemical structure of an ionizable lipid is critical for the delivery efficiency of the LNPs. Herein, we synthesize a new ionizable lipid containing fluorinated alkyl chains (F-L319) and evaluate its mRNA delivery efficiency compared to its hydrocarbon counterpart (L319). While LNPs formulated with F-L319 alone showed decreased mRNA encapsulation and delivery efficiencies in comparison to the L319-LNP, we found that combining the appropriate ratios of F-L319 and L319 as hybrid ionizable lipids in LNPs (hybrid-LNPs) greatly enhanced mRNA delivery efficiency both *in vitro* and *in vivo*. Upon intravenous injection, the hybrid-LNP showed targeted mRNA expression in the spleen. Mechanistic studies indicate that the enhanced mRNA delivery of the hybrid-LNP is attributed to both improved mRNA encapsulation and cellular uptake. Collectively, fluorination of ionizable lipids represents a promising strategy to improve the delivery efficiency of LNPs.



## Introduction

Messenger RNA (mRNA) is an important part of the central dogma of molecular biology.[1] Once exogenous mRNA is delivered into the cytosol of cells, mRNA can express encoded proteins that can serve as therapeutics or vaccines.[2–4] There has long been interest in developing mRNA-based drugs. However, the physiochemical and biological properties of mRNA create great challenges for its translation. mRNA cannot pass through the cell membrane due to its negative charge, hydrophilicity, and large molecular weight. Additionally, naked mRNA is rapidly degraded by enzymes in biological media.[5] Therefore, mRNA requires delivery vehicles to transport it into cells and improve its stability.[6] Among different classes of delivery vehicles, lipid nanoparticles (LNPs) are currently the only carrier for mRNA that receives regulatory approval.[7] The two coronavirus 2019 (COVID-19) mRNA vaccines manufactured by both Moderna and Pfizer/BioNTech used LNPs as carriers and have demonstrated great efficacy and good safety profiles in clinics.[8–10]

LNPs are formulated with an ionizable lipid, a helper lipid, cholesterol, and a polyethylene glycol (PEG)-lipid. Among these components, the chemical structure of ionizable lipids significantly affects the delivery efficiency of mRNA.[11,12] Ionizable lipids are composed of hydrophobic alkyl tails and one or several amino head groups that have an acid dissociation constant ($pK_a$) of less than 7.[13] Ionizable lipids are positively charged in the acidic buffer to interact with negatively charged mRNA to form LNPs, then turn into uncharged at physiological pH to avoid rapid clearance in the systemic circulation, and finally turn into positively charged in the endosome of cells to facilitate mRNA release. The development of ionizable lipids alleviates the toxicity and unwanted interactions with cellular components of cationic lipids. A variety of ionizable lipids have been developed and shown good efficiency in delivering mRNA.[14–17] Despite this progress, new ionizable lipids with improved delivery efficiency are still very much needed to reduce the toxicity and immunogenicity associated with mRNA and LNPs.

Fluorinated lipids, polymers, and dendrimers showed enhanced delivery efficiency compared to non-fluorinated materials for a variety of biologics including DNA, RNA, proteins, *etc.*[18–23] Such an enhanced delivery efficiency was attributed to the unique properties of fluorocarbons. Fluorocarbons

[a] Beijing National Laboratory for Molecular Sciences, CAS Key Laboratory of Colloid, Interface and Chemical Thermodynamics, Institute of Chemistry, Chinese Academy of Sciences, Beijing 100190, China. E-mail: xueguang@iccas.ac.cn; Tel: +86-10-62584391
[b] University of Chinese Academy of Sciences, Beijing 100049, China
[c] State Key Laboratory of Chemical Resource Engineering, Department of Organic Chemistry, College of Chemistry, Beijing University of Chemical Technology, Beijing 100029, China. E-mail: chenning@mail.buct.edu.cn
[d] Key State Laboratory of Fine Chemicals, School of Bioengineering, Dalian University of Technology, Dalian 116024, China. E-mail: jqlin@dlut.edu.cn

† Electronic supplementary information (ESI) available. See DOI: https://doi.org/10.1039/d3tb00516j

‡ These authors contributed equally.

are both hydrophobic and lipophobic, more surface active, stable, and prone to self-assembly compared to hydrocarbons.[24–26] Several studies demonstrated that fluorinated lipids or polymers form more stable nanoparticles, thus preventing the degradation of encapsulated biologics and extending the blood circulation time.[27,28] Therefore, we hypothesized that fluorination of ionizable lipids could be a promising strategy to improve the mRNA delivery efficiency of LNPs.

Herein, we synthesize a new ionizable lipid with highly fluorinated alkyl tails. We found that combining the appropriate ratios of the fluorinated ionizable lipid and its hydrocarbon counterparts in LNPs greatly enhanced mRNA delivery efficiency compared to LNPs that were formulated with only the nonfluorinated ionizable lipid. Mechanistic studies indicate that such an enhanced delivery efficiency was attributed to improved mRNA encapsulation and cellular uptake. Upon intravenous injections in mice, LNPs containing fluorinated lipids showed effective mRNA expression in the spleen.

## Materials and methods

### Materials and instruments

Chemicals were purchased from Beijing Innochem Science & Technology unless noted specifically. 1,2-Distearoyl-*sn*-glycero-3-phosphocholine (DSPC) and 1,2-dimyristoyl-rac-*glycero*-3-methoxypolyethylene glycol-2000 (DMG-PEG 2000) were purchased from Avanti Polar Lipids. Cholesterol was purchased from Sigma-Aldrich. mRNA encoding firefly luciferase (mLuc) was purchased from ApexBio. Di((*Z*)-non-2-en-1-yl)-9-((4-(dimethylamino)butanoyl)oxy)heptadecanedioate (L319) was purchased from WuXi AppTec. Nuclear magnetic resonance (NMR) spectra were recorded using a Bruker Advance II 400 MHz NMR spectrometer with deuterated chloroform ($CDCl_3$) and dimethyl sulfoxide-$d_6$ (DMSO-$d_6$) as solvents with tetramethylsilane (TMS) as the internal standard. Electrospray ionization high-resolution mass spectrometry (ESI-HRMS) measurements were carried out using an Agilent Infinity Lab LC/MSD time-of-flight mass spectrometer.

**Xueguang Lu**

*Dr Xueguang Lu is currently a principal investigator at the Institute of Chemistry, Chinese Academy of Sciences, where his research team focused on nucleic acid-based vaccines and therapeutics for treating infectious diseases and cancer. He received his BS degree in Chemistry from the Beijing University of Chemical Technology under the supervision of Prof. Jiaxi Xu. He then obtained his PhD in Chemistry under the guidance of Prof. Ke Zhang from Northeastern University (Boston). He completed his postdoctoral fellowship at the Massachusetts Institute of Technology, working with Prof. Robert Langer.*

### Synthesis of nonadeca-1,18-dien-10-ol (2)

Magnesium powder (14.4 g, 0.6 mol, 3 eq.) was added to a vacuum flame-dried 500 mL three-necked flask equipped with a Teflon-coated magnetic stir bar. A 100 mL addition funnel and a condenser were equipped and the whole apparatus was exchanged with nitrogen for three times. 100 mL of anhydrous tetrahydrofuran (THF) was injected into the flask and a solution of 9-bromonon-1-ene (42 g, 0.204 mol, 1 eq.) in THF (50 mL) was injected into the addition funnel. The reaction mixture was stirred and heated slowly to 60 °C. 1 mL of iodine (~10 mg) in THF was injected into the system. 9-Bromonon-1-ene in THF was added dropwise at a rate of ~1 drop per second. After the addition of 9-bromonon-1-ene, the reaction was refluxed for 12 h. After cooling with water (~20 °C), a solution of ethyl formate (HCOOEt; 7.4 g, 0.09 mol, 0.9 eq.) in THF (50 mL) was injected to the addition funnel and was then added dropwise to the system. The reaction solution was then refluxed for 12 h. After cooling to room temperature (r. t.), the reaction was quenched by 100 mL of saturated ammonium chloride ($NH_4Cl$) solution and then filtered. The filtrate was evaporated *in vacuo* to remove THF and the residual aqueous solution was extracted twice with ethyl acetate (EtOAc; 200 mL) and then twice with petroleum ether (PE; 200 mL). The organic phase was combined and dried over anhydrous $Na_2SO_4$. After the removal of the solvent *in vacuo*, the residue was dissolved in 30 mL of THF where 30 mL of 40% NaOH was added. The whole system was stirred at 70 °C for 3 h to saponify the esterified product. After cooling to r. t., the reaction system was extracted with EtOAc (30 mL) for three times. The organic phase was collected and dried *in vacuo*. The residue was purified by vacuum distillation to obtain nonadeca-1,18-dien-10-ol at 178–180 °C (2 mmHg using a vacuum gauge) as a sticky oil which soon solidified to a white solid (16.5 g) in 65.4% yield, m.p. 38 °C, $R_f$ = 0.38 (PE:EtOAc = 9 : 1, *v*/*v*). $^1$H NMR (400 MHz, $CDCl_3$) $\delta$ 5.83 (ddt, $J$ = 16.8, 10.2, 6.8 Hz, 2H), 5.08–4.88 (m, 4H), 3.60 (m, 1H), 2.17–1.96 (m, 4H), 1.56–1.19 (m, 24H). $^{13}$C NMR (101 MHz, $CDCl_3$) $\delta$ 139.2, 114.1, 72.0, 37.5, 33.8, 29.7, 29.5, 29.1, 28.9, 25.7.

### Synthesis of nonadeca-1,18-dien-10-yl 4-bromobutanoate (3)

A flame-vacuum dried 250 mL three-necked flask was charged with a magnetic stir bar and a 25 mL addition funnel. The whole apparatus was evacuated and refilled with nitrogen for three times. Nonadeca-1,18-dien-10-ol (16.50 g, 58.82 mmol, 1 eq.) was dissolved in 100 mL of dichloromethane ($CH_2Cl_2$) which was then injected into the flask along with 4 mL of triethylamine ($Et_3N$). 4-Bromobutyryl chloride (14.54 mL, 118 mmol, 2 eq.) was injected into the addition funnel and the whole solution was then added dropwise to the reaction mixture (2 drops per second) in an ice-water bath. After the addition, the reaction system was stirred at r. t. (~20 °C) for 8 h. The organic phase was washed twice with saturated sodium bicarbonate solution ($NaHCO_3$, 100 mL). The organic phase was collected and dried over anhydrous $Na_2SO_4$. After removing the

 

solvent *in vacuo*, the residue was purified by column chromatography with gradient elution (pure PE to PE:EtOAc = 30 : 1), yielding 18.202 g of light yellow oil, 72.0%, $R_f$ = 0.52 (PE/EtOAc = 9 : 1, *v*/*v*). $^1$H NMR (400 MHz, $CDCl_3$) $\delta$ 5.83 (ddt, $J$ = 16.8, 10.2, 6.8 Hz, 2H), 5.01 (dq, $J$ = 16.8, 1.6 Hz, 2H), 4.94 (ddt, $J$ = 10.2, 1.6, 2.4 Hz, 2H), 4.89 (p, $J$ = 6.4 Hz, 1H), 3.49 (t, $J$ = 6.8 Hz, 2H), 2.51 (t, $J$ = 7.2 Hz, 2H), 2.19 (quint, $J$ = 6.8 Hz, 2H), 2.06 (q, $J$ = 6.8 Hz, 4H), 1.56–1.19 (m, 24H). $^{13}$C NMR (101 MHz, $CDCl_3$) $\delta$ 172.3, 139.2, 114.2, 74.7, 34.6, 33.7, 32.8, 32.7, 29.9, 29.4, 29.0, 28.9, 27.9, 25.3.

### Synthesis of 9-((4-bromobutanoyl)oxy)heptadecanedioic acid (4)

Nonadeca-1,18-dien-10-yl 4-bromobutanoate (1.00 g, 2.33 mmol, 1 eq.), 40 mL of $CH_2Cl_2$, 40 mL of acetonitrile ($CH_3CN$), and ruthenium trichloride trihydrate ($RuCl_3{\cdot}3H_2O$; 30 mg, 0.0233 mmol, 1 mol%) were added to a 250 mL flask. Sodium periodate ($NaIO_4$; 4.98 g, 23.3 mmol, 10 eq.) was dissolved in 50 mL of deionized water which was added dropwise (1 drop per second) to the system through an addition funnel in a cold-water bath (0–10 °C). The reaction system was stirred at 0–10 °C until the reactant was consumed by the trace of TLC ($\sim$4 h). The reaction system was washed with saturated sodium thiosulfate solution ($Na_2S_2O_3$; 80 mL) for three times until the color of the aqueous phase changed from dark green to almost colorless. The organic phase was collected and dried over anhydrous $Na_2SO_4$, and the solvent was removed *in vacuo* to obtain the crude 9-((4-bromobutanoyl)oxy)heptadecanedioic acid as a black oil which could be used directly for the next step without further purification, 0.962 g, 85.6%. $R_f$ = 0.62 (DCM:MeOH = 20 : 1, *v*/*v*). $^1$H NMR (400 MHz, DMSO-$d_6$) $\delta$ 11.61 (m, 2H), 4.80 (quint, $J$ = 6.4 Hz, 1H), 3.53 (t, $J$ = 6.4 Hz, 2H), 2.44 (t, $J$ = 7.2 Hz, 2H), 2.18 (t, $J$ = 7.2 Hz, 4H), 2.05 (p, $J$ = 6.4 Hz, 2H), 1.48 (m, 8H), 1.24 (br s, 16H). $^{13}$C NMR (101 MHz, DMSO-$d_6$) $\delta$ 174.9, 172.2, 74.0, 34.3, 34.1, 34.0, 32.7, 29.2, 29.1, 29.0, 28.2, 25.2, 25.0.

### Synthesis of 9-((4-(dimethylamino)butanoyl)oxy)heptadecanedioic acid (5)

9-((4-Bromobutyryl)oxy)heptadecanedioic acid (465.43 mg, 1 mmol, 1 eq.), dimethylamine tetrahydrofuran (2 M; 5 mL, 10 mmol), and potassium carbonate ($K_2CO_3$; 304.05 mg, 2.2 mmol, 2.2 eq.) were added to a pressure tube. The reaction mixture was heated at 50 °C for 8 h. A white precipitate was observed in the pressure tube. After cooling to r. t., acetic acid or HCl (1 M) was added dropwise until the white precipitate dissolved (pH 6–7). 5 mL of water was added before extraction with $CH_2Cl_2$ (10 mL) for three times. The organic phase was combined and then washed with saturated brine solution (10 mL). The organic phase was collected and dried over anhydrous $Na_2SO_4$. After removing the solvent *in vacuo*, the crude 9-((4-(dimethylamino)butanoyl)oxy)heptadecanedioic acid was obtained as a yellowish oil which could be used directly for the next step without any further purification, 356 mg, 82.9%. $R_f$ = 0.21 (DCM:MeOH = 10 : 1, *v*/*v*).

### Synthesis of bis(2,2,3,3,4,4,5,5,6,6,7,7,8,8,9,9-hexadecafluorononyl) 9-((4-(dimethylamino)butanoyl)oxy)heptadecanedioate (F-L319)

9-((4-(Dimethylamino)butanoyl)oxy)heptadecanedioic acid (42.96 mg, 0.1 mmol, 1 eq.), $CH_2Cl_2$ (5 mL), and 4-(*N*,*N*-dimethylamino)pyridine (DMAP; 6.11 mg, 0.05 mmol, 0.5 eq.) were added to a 25 mL flask. The reaction mixture was stirred at r. t. for 30 min, followed by the addition of 1-(3-dimethylaminopropyl)-3-ethylcarbodiimide hydrochloride (EDCI; 42.17 mg, 0.22 mmol, 2.2 eq.). The reaction system was stirred for 15 min. 1*H*,1*H*,9*H*-hexadecafluorononanol (95.06 mg, 0.22 mmol, 2.2 eq.) was added and the whole system was stirred at r. t. overnight ($\sim$10 h). The reaction system was sequentially washed with $NH_4Cl$ (5 mL), deionized water (5 mL), and saturated brine (5 mL). The organic phase was collected and dried over anhydrous $Na_2SO_4$. After removing the solvent *in vacuo*, the residue was purified by column chromatography (DCM:MeOH:$Et_3N$ = 100 : 10 : 1, *v*/*v*) to yield yellow oil, 38 mg, 30%, $R_f$ = 0.86 (DCM). $^1$H NMR (400 MHz, $CDCl_3$) $\delta$ 6.27–5.92 (m, 2H), 4.86 (quint, $J$ = 6.4 Hz, 1H), 4.61 (t, $J$ = 13.6 Hz, 4H), 2.93 (m, 2H), 2.68 (s, 6H), 2.43 (m, 6H), 2.10 (quint, $J$ = 6.8 Hz, 2H), 1.65 (m, 4H), 1.39–1.28 (m, 20H). $^{19}$F NMR (377 MHz, $CDCl_3$) $\delta$ −119.48, −121.94, −123.29, −129.27, −136.97. $[M + H]^+$, exact mass: 1258.2971, found mass: 1258.2991.

### Cell culture

Murine dendritic cells (DC2.4) and mouse macrophage 264.7 cell line (RAW264.7) were cultured in the Roswell Park Memorial Institute (RPMI) 1640 medium (Gibco) supplemented with 10% fetal bovine serum (Gibco) and 1% penicillin/streptomycin (Gibco) at 37 °C in the presence of 5% $CO_2$.

### Synthesis of LNPs

LNPs were synthesized by mixing the lipids and mLuc in a microfluidic chip. Briefly, ionizable lipids (F-L319, L319, and combined), DSPC, cholesterol, and DMG-PEG2000 at a molar ratio of 50 : 10 : 38.5 : 1.5, respectively, were dissolved in the ethanol phase. mLuc or cyanine-5 (Cy5)-labeled oligonucleotide (5′-GCTATTAGGAGGAGTCTTT–Cy5–3′) was dissolved in 50 mM citrate buffer (pH = 4). The ratio of nitrogen on ionizable lipids to the phosphate of mRNA is 5.67 : 1. The ethanol phase and aqueous phase were mixed with a volume ratio of 3 : 1 using syringe pumps (Harvard Apparatus). The mixture was dialyzed (MWCO = 12 k–14 kDa, Biorigin) against phosphate-buffered saline (PBS) at r. t. for over 4 h. The hydrodynamic diameter and polydispersity index (PDI) of LNPs were measured at 25 °C using a Zetasizer Nano ZSP (Malvern Instruments). The encapsulation efficiency was measured using Quant-iT RiboGreen RNA assay (Thermo Fisher Scientific) according to the manufacturer's instructions. The p$K_a$ of LNP was measured using the 6-(*p*-toluidino)-2-napthalenesulfonic acid sodium salt (TNS, Sigma-Aldrich) assay following a previously published method.[29]

### *In vitro* transfection of lipid nanoparticles

To evaluate the mRNA delivery efficiency *in vitro*, DC2.4 cells or RAW264.7 cells were seeded at a density of $2 \times 10^4$ cells per well

in a Corning™ Costar™ 96-well plate. After incubation at 37 °C overnight, LNPs containing 100 ng of mRNA were added to each well. After incubation at 37 °C for 12 h or 24 h, a One-lite Luciferase Assay substrate in 100 μL of lysis buffer was added to each well. The luminescence was then read using a BioTek Synergy H1 multimode microplate reader (Agilent). To study the cellular uptake of LNPs, LNPs encapsulating Cy5-DNA were incubated with DC2.4 cells at 37 °C for 3 h. Cells were then digested with 0.25% trypsin, washed three times with PBS, and analyzed using a CytoFLEX flow cytometer (Beckman Coulter). For confocal analysis, cells were washed twice with 1× PBS after incubating with LNPs. To label the cell nucleus, the cells were further incubated with Hoechst for 15 min. Cells were washed twice with 1× PBS before being fixed with 4% paraformaldehyde for 15 minutes. The fixed cells were then imaged by confocal laser scanning microscopy (CLSM).

### *In vitro* cytotoxicity assay

DC 2.4 cells were incubated with LNPs with different concentrations of mRNA for 12 h. The medium containing LNPs was then replaced with a culture medium. The cell viability was measured using the cell counting kit-8 (CCK-8) assay according to the manufacturer's instructions (Vazyme). The results were measured using a microplate reader (BioTek Synergy H1) at 450 nm.

### *In vivo* delivery efficiency of LNPs

All animal experiments reported here were performed according to a protocol approved by the Peking University Institutional Animal Care and Use Committee. 6–8 Weeks C57BL/6 female mice were intravenously administered with LNPs at a dose of 2 μg of mLuc per mouse through the tail vein. Mice were anesthetized using isoflurane and 200 μL of potassium (*S*)-2-(6-hydroxybenzo[d]thiazol-2-yl)-4,5-dihydrothiazole-4-carboxylate (Bidepharm, 20 mg $mL^{-1}$) was administered through intraperitoneal injections. The mice were then imaged using an *in vivo* imaging system (IVIS Spectrum, PerkinElmer) to quantify bioluminescence signals. At 24 h post-injection of LNPs, the major organs of mice were excised and imaged by IVIS to determine the biodistribution of mRNA expression.

### Hemolysis of red blood cells

The hemolysis of red blood cells (RBCs) was performed according to a previously published method.[30] Briefly, mouse RBCs were isolated from mouse blood by centrifugation at 300 × *g* for 5 min. RBCs were washed three times with PBS and suspended in PBS at a pH of 5.5 or 7.4. 200 μL of RBC solution was added to each well of a 96-well plate. LNPs containing 200 ng of mRNA or 0.1% Triton-X100 were added to each well and incubated at 37 °C for 1 h. The plate was centrifuged at 300 × *g* at 4 °C for 5 min. 100 μL of aliquot from each well was transferred to a transparent 96-well plate. The absorbance at 540 nm of each well was measured using a BioTek Synergy H1 multimode microplate reader (Agilent).

## Results and discussion

### Synthesis of bis(2,2,3,3,4,4,5,5,6,6,7,7,8,8,9,9-hexadecafluorononyl) 9-((4-(dimethylamino)butanoyl)oxy)heptadecanedioate (F-L319)

Dlin-MC3-DMA (MC-3) is a potent ionizable lipid that has gained regulatory approval in the first clinically approved small interfering RNA drug (patisiran by Alnylam).[31] A biodegradable version of MC-3 termed as L319 bearing an ester group on each alkyl chain was then developed.[32] To test our hypothesis, we synthesized fluorinated L319 as an ionizable lipid (F-L319) and compared its mRNA delivery efficiency with nonfluorinated L319. F-L319 was synthesized in 5 steps as shown in Fig. 1A under modified reaction conditions compared to the published synthetic method of L319.[32] The lengths of the lipid tails of L319 and F-L319 are the same. Each of the intermediates was characterized by $^{1}$H NMR and $^{13}$C NMR spectroscopies (Fig. S1–S3, ESI†). During the last step of the synthesis, 1*H*,1*H*,9*H*-hexadecafluorononanol instead of non-2-en-1-ol was reacted with 9-((4-(dimethylamino)butanoyl)oxy)heptadecanedioic acid (compound **5**) to yield F-L319. The overall yield of F-L319 is ∼10% after 5 steps. $^{1}$H NMR, $^{19}$F NMR, and Fourier-transform infrared (FT-IR) spectroscopies and high-resolution mass spectrometry demonstrated the successful synthesis of F-L319 with high purity (Fig. 1B, C and Fig. S4, S5, ESI†).

### Synthesis and characterization of LNPs

To test whether F-L319 could form LNPs with non-fluorinated helper lipids, we used the same formulation as the COVID-19 mRNA vaccine by Moderna. F-L319, 1,2-distearoyl-*sn*-glycero-3-phosphocholine (DSPC), cholesterol, and 1,2-dimyristoyl-rac-*glycero*-3-methoxy(polyethylene glycol-2000) (DMG-PEG2000) at a molar ratio of 50 : 10 : 38.5 : 1.5, respectively, were formulated with firefly luciferase mRNA (mLuc) through a microfluidic device to yield the F-L319-LNP (Fig. 2A). The same LNP formulation with L319 as the ionizable lipid was also synthesized as a control (L319-LNP). Dynamic light scattering (DLS) measurements show that the hydrodynamic diameter ($D_h$) and polydispersity index (PDI) of F-L319-LNP are ∼245 nm and ∼0.19 (Fig. 2B and C), respectively, which are both higher than those of L319-LNP (∼219 nm and ∼0.14, respectively). F-L319-LNP also exhibits a decreased mRNA encapsulation efficiency (∼21.8%) compared to L319-LNP (∼57.1%, Fig. 2D). These results suggest that the lipophobicity of F-L319 may affect its assembly with non-fluorinated helper lipids, resulting in poor mRNA encapsulation. Therefore, we decreased the amount of F-L319 and prepared LNPs formulated with hybrid ionizable lipids of both L319 and F-L319 (hybrid-LNP). Two ratios of L319 : F-L319 were tested as shown in Table 1. Hybrid-LNPs show decreased $D_h$ and enhanced mRNA encapsulation compared to L319-LNP (Fig. 2B and D). Additionally, higher amounts of F-L319 in hybrid-LNP yield smaller $D_h$ and narrower PDI (Fig. 2B and C). The surface potentials of hybrid-LNPs are higher than those of L319-LNP and F-L319-LNP (Fig. 2E). The overall negative charges of L319-LNP (∼−10 mV) and F-L319-LNP (∼−11 mV) are likely because of the high amount of free

 

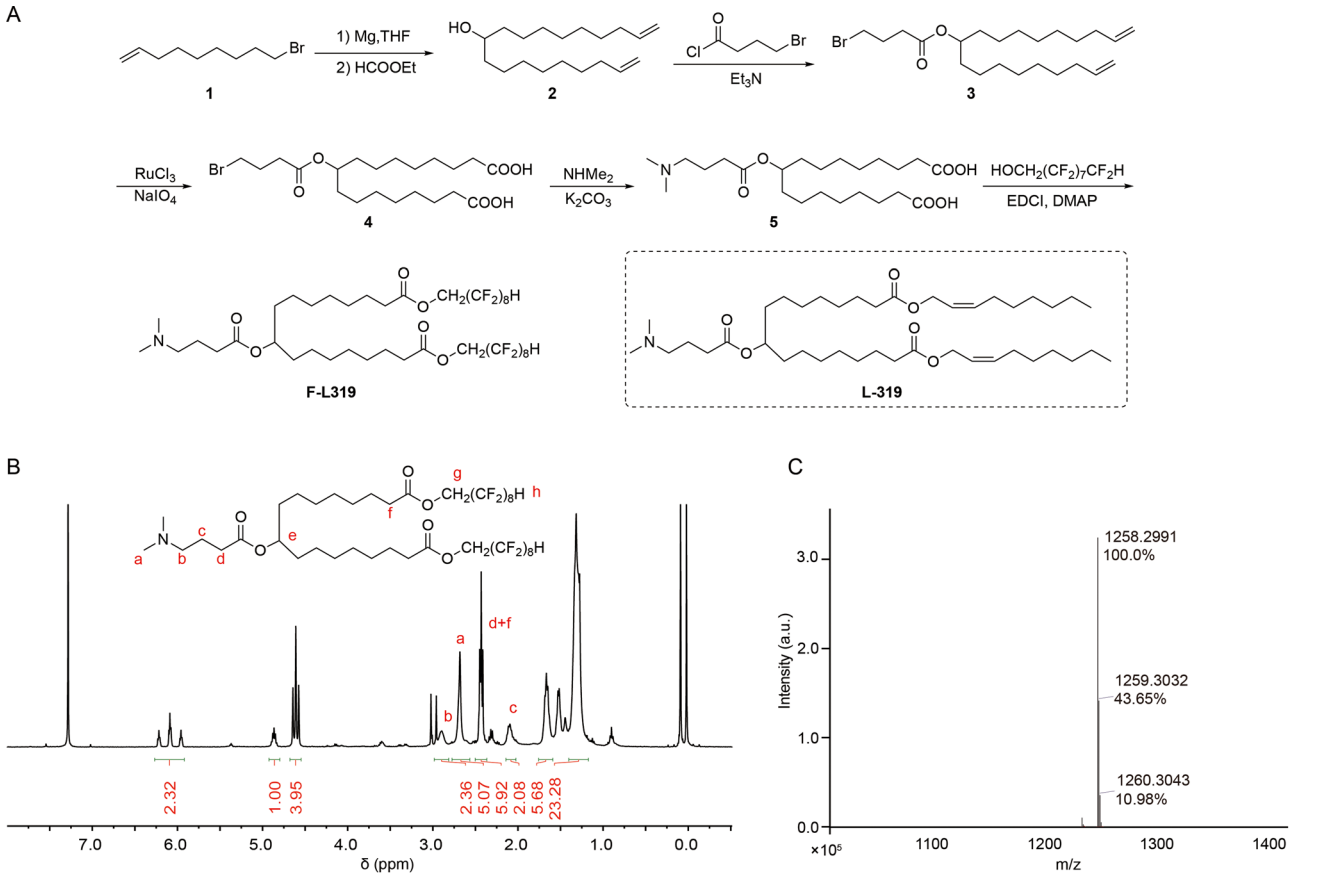


Fig. 1 (A) Synthesis of F-L319. The chemical structure of L319 is shown in the dotted box. The $^{1}$H NMR spectrum (B) and high-resolution mass spectrum (C) of F-L319 (exact mass for $C_{41}H_{48}F_{32}NO_6^+$ [M + H]$^+$: 1258.2971, found: 1258.2991).

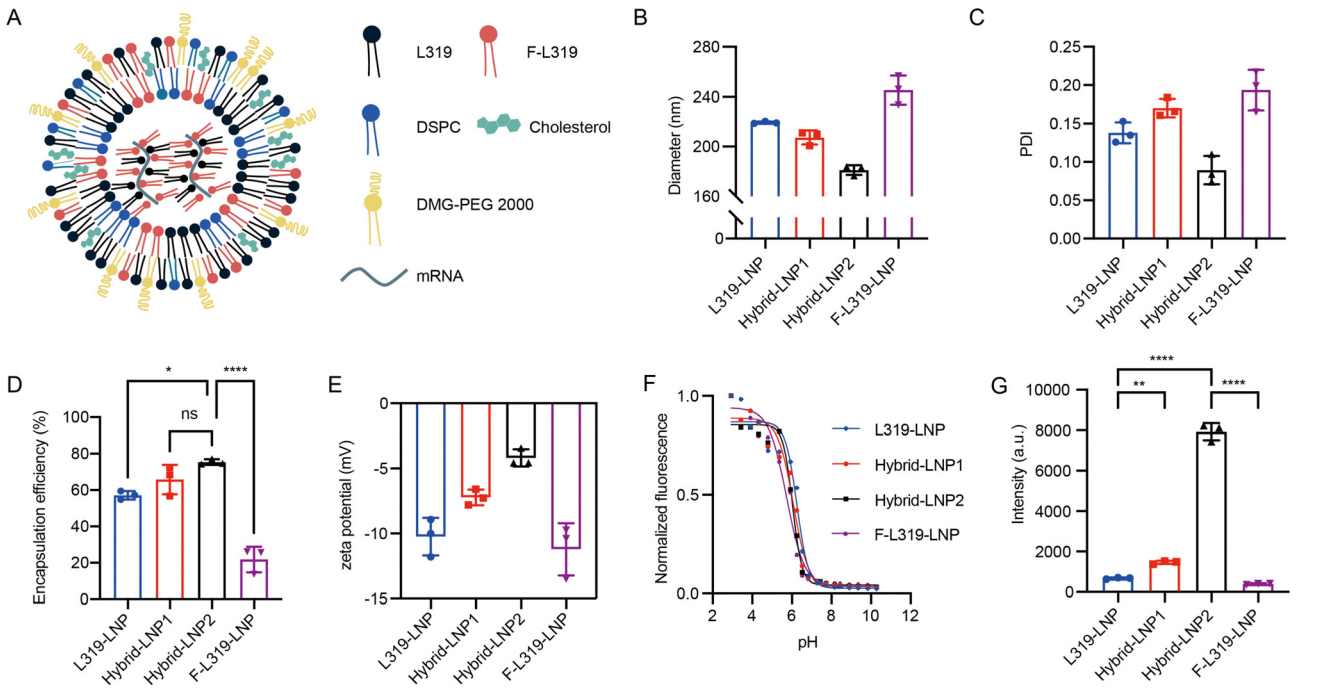


Fig. 2 (A) Schematic view of hybrid-LNPs. The hydrodynamic diameter (B), polydispersity index (C), mRNA encapsulation efficiency (D), and zeta potential (E) of LNPs ($n$ = 3). (F) Determination of p$K_a$ of LNPs using the TNS fluorescence assay. (G) Transfection efficiency of the LNPs after 12 h incubation in DC2.4 cells ($n$ = 3). The statistical significance was calculated by one-way ANOVA: *$p$ < 0.05, **$p$ < 0.01, ****$p$ < 0.001, ns represents not statistically significant.

Table 1 Composition of LNPs. Numbers represent the percentage of molar ratios

| Formulations | L319 | F-L319 | DSPC | Cholesterol | DMG-PEG2000 |
|---|---|---|---|---|---|
| L319-LNP | 50 | 0 | 10 | 38.5 | 1.5 |
| F-L319-LNP | 0 | 50 | 10 | 38.5 | 1.5 |
| Hybrid-LNP1 | 33.3 | 16.7 | 10 | 38.5 | 1.5 |
| Hybrid-LNP2 | 25 | 25 | 10 | 38.5 | 1.5 |

mRNA in the solution due to the poor encapsulation efficiency. The hybrid-LNP2 bearing higher amounts of F-L319 exhibits only slightly higher surface potential than hybrid-LNP1. Hybrid-LNP1 showed a spherical morphology as shown in the transmission electron microscopy image (Fig. S6, ESI†). Collectively, these data showed that hybrid-LNPs have smaller sizes, narrower PDI, and higher mRNA encapsulation efficiency than L319-LNP, suggesting that hybrid-LNPs could be more effective in delivering mRNA.

The p$K_a$ of LNP is critical for its delivery efficiency (*vide supra*). We next tested the p$K_a$ of all LNPs using a 2-(*p*-toluidino) naphthalene-6-sulfonic acid (TNS) assay according to a previously published protocol.[29] As shown in Fig. 2F, L319-LNP has a p$K_a$ of ~6.25, which is consistent with the previously published results.[32] Hybrid-LNP1 and -LNP2 have p$K_a$ values of 6.06 and 6.02, respectively, indicating that F-L319 decreases the p$K_a$ of LNPs. Such an observation is reasonable because the strong electron-withdrawing effect of fluorine could increase the acidity of tertiary amine on adjacent ionizable lipids. Nonetheless, the p$K_a$ values of hybrid LNPs are still within the optimal range for mRNA delivery.[33] F-L319-LNP has the lowest p$K_a$ value (5.73) among all LNPs. Collectively, these data suggest that all LNPs maintained the ideal p$K_a$ for efficient mRNA delivery.

### *In vitro* and *in vivo* delivery efficiencies of LNPs

We next evaluated the *in vitro* delivery efficiency of LNPs. LNPs encapsulating mLuc were incubated with DC2.4 cells for 12 h before measuring luciferase activity. L319-LNP treatment shows low luciferase signals suggesting the ineffective delivery of mRNA (Fig. 2G), which is consistent with published results.[34] In contrast, both hybrid-LNPs exhibit enhanced luciferase expressions than L319-LNP. Hybrid-LNP1 shows a ~2.2-fold higher mRNA expression than L319-LNP. Hybrid-LNP2 shows the highest mRNA expression, which is ~11.7-fold and ~5.4-fold higher than that of L319-LNP and hybrid-LNP1, respectively, suggesting that higher amounts of F-L319 contributed to the increased delivery efficiency of mRNA. F-L319-LNP has the lowest luciferase signal, probably due to the poor mRNA encapsulation efficacy. Similar results were observed when LNPs were incubated with cells for 24 h (Fig. S7, ESI†).

We next validated the enhanced delivery efficiency of hybrid-LNPs *in vivo*. We first tested the cytotoxicity of LNPs before injecting LNPs in mice. L319 is the biodegradable derivative of MC-3, which is already approved for the clinical use. Therefore, we do not anticipate the significant toxicity of L319 or F-L319. Indeed, all LNPs did not show apparent toxicity at all tested concentrations (Fig. S8, ESI†). After demonstrating the safety profiles, LNPs encapsulating mLuc were intravenously administered into female C57BL/6 mice at a dose of 2 μg of mRNA per mouse. The mice were then imaged at different time points post-injection using an *in vivo* live imaging system. As shown in Fig. 3A, L319-LNP and hybrid LNPs show rapid mRNA expression with strong luminescence signals at 4 h post-injection. The luminescence signal decreases gradually from 4 h to 24 h indicating the transient expression of mRNA (Fig. S9, ESI†). Even though hybrid-LNP2 has significantly higher mRNA expression than hybrid-LNP1 *in vitro*, *in vivo* imaging shows that both hybrid-LNPs exhibit comparable luminescence signals, which are both higher than L319-LNP and F-L319-LNP at all tested time points. These results further support the notion that *in vitro* results are poor predictors of the *in vivo* delivery efficacy of LNPs.[5] The differences between mRNA expression *in vitro* and *in vivo* could be due to different mRNA expressions in different cells. We observed similar *in vitro* delivery efficacy of hybrid-LNP1 and hybrid-LNP2 using a mouse macrophage 264.7 cell line (Fig. S10, ESI†). F-L319-LNP barely exhibits any mRNA expression *in vivo*. Quantification analysis shows that hybrid-LNP2 produces stronger luciferase signals than hybrid-LNP1 at 4 h post-injection. However, the luminescence of hybrid-LNP2 declines more rapidly than that of hybrid-LNP1 (Fig. 3B). Such an observation could be due to the decreased colloidal stability of hybrid-LNP2, which has a higher amount of F-L319 than that of hybrid-LNP1. Collectively, these results demonstrated that hybrid-LNPs exhibit significantly higher mRNA delivery efficiency than L319-LNP *in vivo.*

To further evaluate mRNA expression in different organs, mice were euthanized at 24 h post-injection for *ex vivo* imaging. Fig. 3C shows that hybrid-LNPs and L319-LNP exhibit similar profiles with the most mRNA expression in the spleen. Much weaker mRNA expression in the liver and nearly no expression in other major organs were observed from *in vivo* and *ex vivo* imaging results. The majority of the previously published LNPs showed the strongest mRNA expression in the liver after intravenous injections. Interestingly, L-319-LNP and F-L319-LNP showed targeted expression in the spleen. Siegwart *et al.* recently found that negatively charged LNPs showed the spleen-targeted mRNA expression.[16] As shown in Fig. 2E, hybrid-LNPs and L319-LNP all exhibit overall negative charges, which could be the reason for their targeted mRNA expression in the spleen. However, the mechanism of the unique distribution profile of hybrid-LNPs requires further investigation. Collectively, these results demonstrate that incorporating F-L319 in LNPs enhances mRNA delivery efficiency *in vivo*. Hybrid-LNPs showed targeted mRNA expression in the spleen. Completely replacing L319 with F-L319 in LNPs results in poor encapsulation and delivery efficiencies.

### Cellular uptake of LNPs

Previous studies showed that fluorinated lipids or polymers enhanced the cellular uptake of their hydrocarbon counterparts.[18,19] To explore the mechanism of the enhanced delivery efficiency of hybrid-LNPs, we first studied their ability to enter cells. A Cyanine 5-labeled oligonucleotide strand (Cy5-DNA) was

 

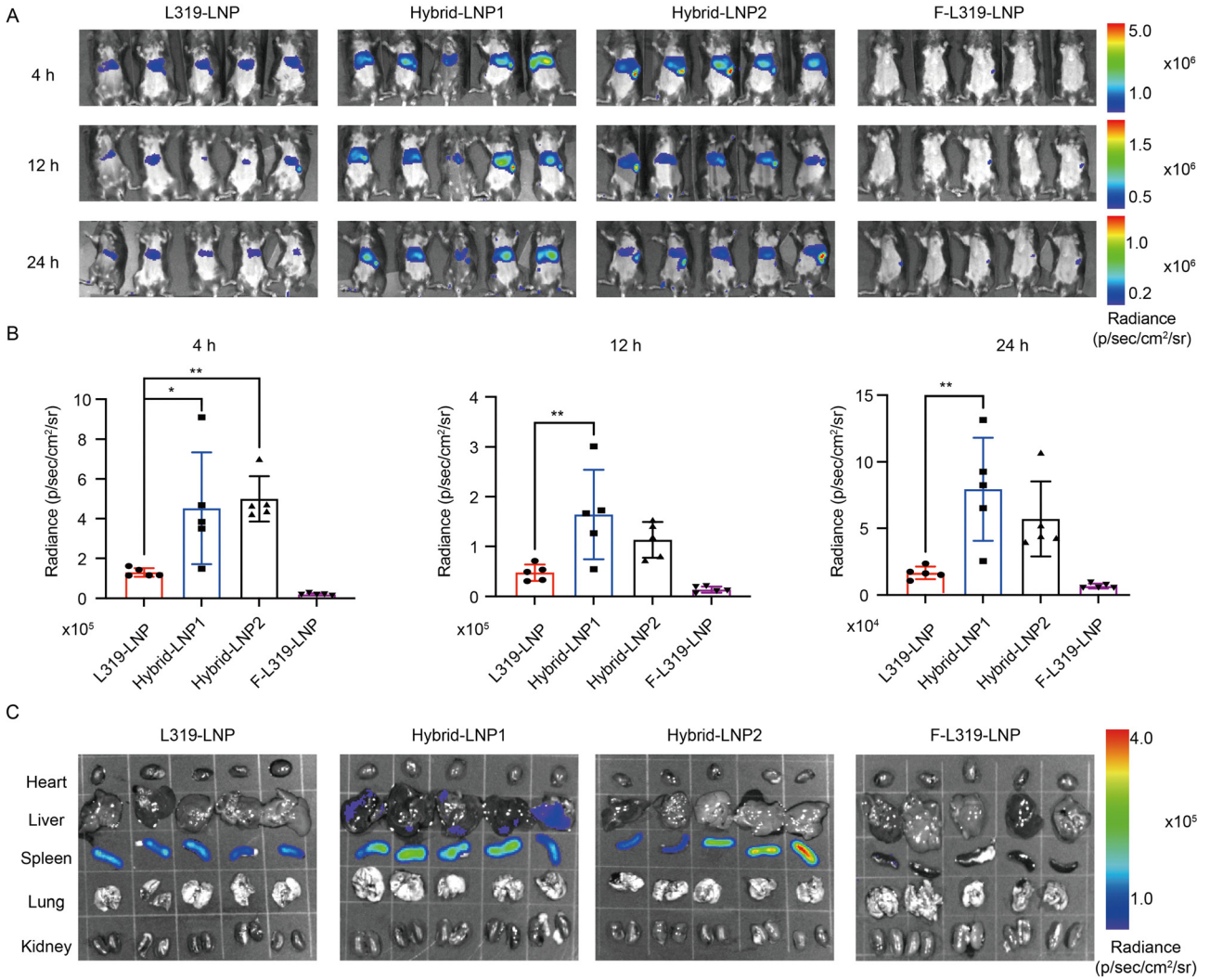


Fig. 3 (A) Representative IVIS images of mice at 4 h, 12 h, and 24 h post intravenous injection of LNPs (2 μg of mLuc per mouse). (B) Quantification of bioluminescence signals of mice ($n$ = 5 biologically independent samples). The statistical significance was calculated by one-way ANOVA: *$p < 0.05$, **$p < 0.01$. (C) *Ex vivo* images of major organs from mice treated with LNPs (n = 5 biologically independent samples). Mice were euthanized at 24 h post injection of LNPs.

encapsulated in LNPs to enable the quantification of LNPs in cells. DC2.4 cells were incubated with LNPs for 3 h before flow cytometry analysis. Free Cy5-DNA was used as a control. All LNPs show greatly enhanced cellular uptake than free Cy5-DNA as shown in Fig. 4A and B. Hybrid-LNPs are internalized by cells at nearly identical amounts, which are ~1.4-fold higher than L319-LNP. F-L319-LNP shows lower cellular uptake than L319-LNP, possibly due to the poor encapsulation efficiency. Confocal laser scanning microscopy further confirms the enhanced cellular uptake of hybrid-LNPs. As shown in Fig. 4C and Fig. S11 (ESI†), hybrid-LNPs produce much stronger fluorescence signals in the cytosol of cells than L319-LNP. Collectively, these results indicate that hybrid-LNPs have better cellular uptake ability than L319-LNP, which contributes to their improved mRNA delivery efficiency.

### Hemolysis induced by LNPs

In addition to cellular uptake, endosomal escape is another important parameter that determines the mRNA delivery efficiency. The efficacy of endosomal escape is partially correlated to the membrane fusion of LNPs.[30,35] To investigate the membrane fusion of LNPs, we incubated LNPs with red blood cells (RBCs) of mice at acidic and neutral pHs. Non-treated RBCs and 0.1% Triton X-100 were used as the negative and positive controls. The hemolysis of RBCs is positively correlated to the membrane fusion of LNPs. All LNPs show nearly no hemolysis at pH 7.4 because ionizable lipids are not protonated (Fig. 5). At pH 5.5, which is below the p$K_a$ of all LNPs, L319-LNP exhibits significantly higher hemolytic ability than hybrid-LNPs. F-L319-LNP shows the lowest fusion with RBCs. These results indicate that F-L319 has lower membrane fusion ability than L319. The incorporation of F-L319 into L319-LNP decreases its membrane fusion ability. This is reasonable because the lipophobicity of F-L319 inhibits its interaction with alkyl lipids on the cell membrane. Collectively, the enhanced encapsulation and cellular uptake of hybrid-LNPs compensated for their

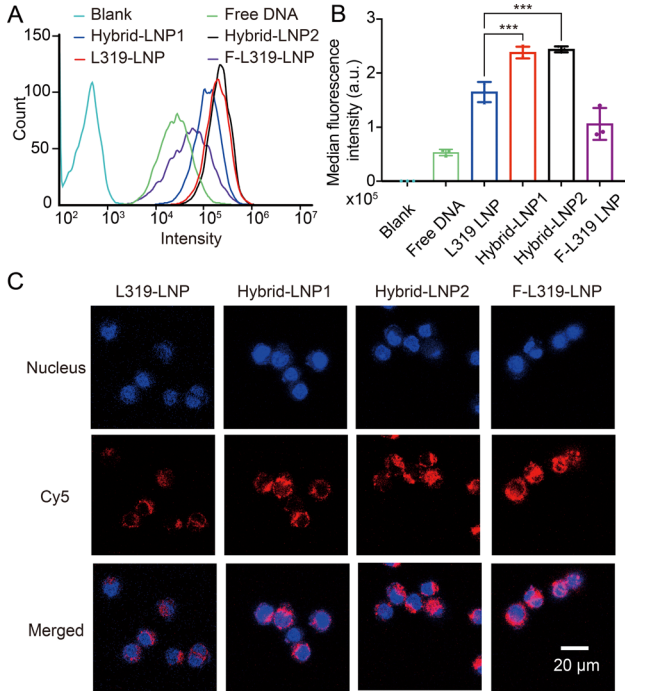


Fig. 4 Flow cytometry plots (A) and quantitative analysis (B) of DC2.4 cells treated with Cy5-LNPs ($n$ = 3). The statistical significance was calculated by one-way ANOVA: ***$p < 0.001$. (C) Confocal fluorescence microscopy images of DC2.4 cells treated with LNPs.

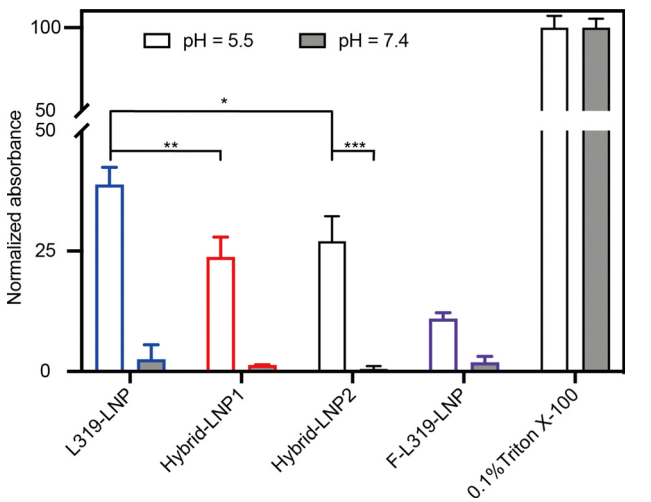


Fig. 5 Hemolysis of RBCs after incubation with LNPs at pH 5.5 or 7.4 ($n$ = 3). The statistical significance was calculated by Student's $t$ test or one-way ANOVA: *$P < 0.05$, **$P < 0.01$, ***$P < 0.001$, ns represents not statistically significant.

decreased membrane fusion, resulting in overall enhanced mRNA delivery efficiency.

## Conclusions

We synthesized a new ionizable lipid containing fluorinated alkyl chains termed F-L319 and evaluated its efficiency in delivering mRNA. LNPs formulated with F-L319 by itself as the ionizable lipid showed reduced encapsulation and delivery efficiencies. Such an observation is due to the poor co-assembly between F-L319 and helper lipids that bear alkyl chains. To alleviate this incompatibility between F-L319 and helper lipids, we formulated hybrid LNPs containing both F-L319 and L319 as ionizable lipids. It is found that hybrid-LNPs significantly enhanced mRNA delivery efficiency compared to the L319-LNP both *in vitro* and *in vivo*. Hybrid-LNPs did not alter the biodistribution profile of the L319-LNP among different organs, with >90% of expression in the spleen after intravenous injection. The mechanistic study showed that the incorporation of F-L319 significantly enhanced the cellular uptake of LNPs, which partially contributed to the overall enhanced mRNA delivery. The present study suggests that modifying the alkyl chains of ionizable lipids with fluorine is a promising strategy to improve the overall mRNA delivery efficiency of LNPs.

## Author contributions

Conceptualization, J. L., N. C., and X. L.; methodology, H. H., X. C., J. X., J. L., N. C., and X. L.; investigation, H. H., X. C., J. X., N. C., J. L., and X. L.; resources, J. X., J. L., N. C., and X. L.; writing—review and editing, J. X., J. L., N. C., and X. L.; supervision, N. C., and X. L.; and funding acquisition, J. L., N. C., and X. L. All authors have read and agreed to the published version of the manuscript.

## Conflicts of interest

There are no conflicts to declare.

## Acknowledgements

This research was supported by the National Natural Science Foundation of China (No. 22175188), and start-up funding from the Institute of Chemistry, Chinese Academy of Sciences.

## Notes and references

1 S. Brenner, F. Jacob and M. Meselson, *Nature*, 1961, **190**(4776), 576–581.
2 J. M. Richner, S. Himansu, K. A. Dowd, S. L. Butler, V. Salazar, J. M. Fox, J. G. Julander, W. W. Tang, S. Shresta, T. C. Pierson, G. Ciaramella and M. S. Diamond, *Cell*, 2017, **168**(6), 1114–1125.
3 X. Hou, X. Zhang, W. Zhao, C. Zeng, B. Deng, D. W. McComb, S. Du, C. Zhang, W. Li and Y. Dong, *Nat. Nanotechnol.*, 2020, **15**(1), 41–46.
4 S. Ramaswamy, N. Tonnu, K. Tachikawa, P. Limphong, J. B. Vega, P. P. Karmali, P. Chivukula and I. M. Verma, *Proc. Natl. Acad. Sci. U. S. A.*, 2017, **114**(10), E1941–E1950.
5 K. Paunovska, D. Loughrey and J. E. Dahlman, *Nat. Rev. Genet.*, 2022, **23**, 265–280.

6 X. Huang, N. Kong, X. Zhang, Y. Cao, R. Langer and W. Tao, *Nat. Med.*, 2022, **28**, 2273–2287.
7 X. Hou, T. Zaks, R. Langer and Y. Dong, *Nat. Rev. Mater.*, 2021, **6**, 1079–1094.
8 F. P. Polack, S. J. Thomas, N. Kitchin, J. Absalon, A. Gurtman, S. Lockhart, J. L. Perez, G. Pérez Marc, E. D. Moreira, C. Zerbini, R. Bailey, K. A. Swanson, S. Roychoudhury, K. Koury, P. Li, W. V. Kalina, D. Cooper, R. W. Frenck, L. L. Hammitt, Ö. Türeci, H. Nell, A. Schaefer, S. Ünal, D. B. Tresnan, S. Mather, P. R. Dormitzer, U. Şahin, K. U. Jansen and W. C. Gruber, *N. Engl. J. Med.*, 2020, **383**(27), 2603–2615.
9 K. S. Corbett, D. K. Edwards, S. R. Leist, O. M. Abiona, S. Boyoglu-Barnum, R. A. Gillespie, S. Himansu, A. Schäfer, C. T. Ziwawo, A. T. DiPiazza, K. H. Dinnon, S. M. Elbashir, C. A. Shaw, A. Woods, E. J. Fritch, D. R. Martinez, K. W. Bock, M. Minai, B. M. Nagata, G. B. Hutchinson, K. Wu, C. Henry, K. Bahl, D. Garcia-Dominguez, L. Z. Ma, I. Renzi, W. P. Kong, S. D. Schmidt, L. Wang, Y. Zhang, E. Phung, L. A. Chang, R. J. Loomis, N. E. Altaras, E. Narayanan, M. Metkar, V. Presnyak, C. Liu, M. K. Louder, W. Shi, K. Leung, E. S. Yang, A. West, K. L. Gully, L. J. Stevens, N. Wang, D. Wrapp, N. A. Doria-Rose, G. Stewart-Jones, H. Ben-nett, G. S. Alvarado, M. C. Nason, T. J. Ruckwardt, J. S. McLellan, M. R. Denison, J. D. Chappell, I. N. Moore, K. M. Morabito, J. R. Mascola, R. S. Baric, A. Carfi and B. S. Graham, *Nature*, 2020, **586**(7830), 567–571.
10 L. A. Jackson, E. J. Anderson, N. G. Rouphael, P. C. Roberts, M. Makhene, R. N. Coler, M. P. McCullough, J. D. Chappell, M. R. Denison, L. J. Stevens, A. J. Pruijssers, A. McDermott, B. Flach, N. A. Doria-Rose, K. S. Corbett, K. M. Morabito, S. O'Dell, S. D. Schmidt, P. A. Swanson, M. Padilla, J. R. Mascola, K. M. Neuzil, H. Bennett, W. Sun, E. Peters, M. Makowski, J. Albert, K. Cross, W. Buchanan, R. Pikaart-Tautges, J. E. Ledgerwood, B. S. Graham and J. H. Beigel, *N. Engl. J. Med.*, 2020, **383**(20), 1920–1931.
11 A. Akinc, A. Zumbuehl, M. Goldberg, E. S. Leshchiner, V. Busini, N. Hossain, S. A. Bacallado, D. N. Nguyen, J. Fuller, R. Alvarez, A. Borodovsky, T. Borland, R. Constien, A. De Fougerolles, J. R. Dorkin, K. Narayanan-nair Jayaprakash, M. Jayaraman, M. John, V. Koteliansky, M. Manoharan, L. Nechev, J. Qin, T. Racie, D. Raitcheva, K. G. Rajeev, D. W. Y. Sah, J. Soutschek, I. Toudjarska, H. P. Vornlocher, T. S. Zimmermann, R. Langer and D. G. A. Anderson, *Nat. Biotechnol.*, 2008, **26**(5), 561–569.
12 L. Miao, L. Li, Y. Huang, D. Delcassian, J. Chahal, J. Han, Y. Shi, K. Sadtler, W. Gao, J. Lin, J. C. Doloff, R. Langer and D. G. Anderson, *Nat. Biotechnol.*, 2019, **37**(10), 1174–1185.
13 K. J. Kauffman, J. R. Dorkin, J. H. Yang, M. W. Heartlein, F. Derosa, F. F. Mir, O. S. Fenton and D. G. Anderson, *Nano Lett.*, 2015, **15**(11), 7300–7306.
14 K. A. Whitehead, J. R. Dorkin, A. J. Vegas, P. H. Chang, O. Veiseh, J. Matthews, O. S. Fenton, Y. Zhang, K. T. Olejnik, V. Yesilyurt, D. Chen, S. Barros, B. Klebanov, T. Novobrantseva, R. Langer and D. G. Anderson, *Nat. Commun.*, 2014, **5**, 4277.
15 M. Qiu, Y. Tang, J. Chen, R. Muriph, Z. Ye, C. Huang, J. Evans, E. P. Henske and Q. Xu, *Proc. Natl. Acad. Sci. U. S. A.*, 2022, **119**(8), 1–10.
16 Q. Cheng, T. Wei, L. Farbiak, L. T. Johnson, S. A. Dilliard and D. J. Siegwart, *Nat. Nanotechnol.*, 2020, **15**(4), 313–320.
17 J. E. Dahlman, C. Barnes, O. F. Khan, A. Thiriot, S. Jhunjunwala, T. E. Shaw, Y. Xing, H. B. Sager, G. Sahay, L. Speciner, A. Bader, R. L. Bogorad, H. Yin, T. Racie, Y. Dong, S. Jiang, D. Seedorf, A. Dave, K. Singh Sandhu, M. J. Webber, T. Novobrantseva, V. M. Ruda, A. K. R. Lytton-Jean, C. G. Levins, B. Kalish, D. K. Mudge, M. Perez, L. Abezgauz, P. Dutta, L. Smith, K. Charisse, M. W. Kieran, K. Fitzgerald, M. Nahrendorf, D. Danino, R. M. Tuder, U. H. Von Andrian, A. Akinc, D. Panigrahy, A. Schroeder, V. Koteliansky, R. Langer and D. G. Anderson, *Nat. Nanotechnol.*, 2014, **9**(8), 648–655.
18 M. Wang, H. Liu, L. Li and Y. Cheng, *Nat. Commun.*, 2014, **5**, 1–8.
19 G. Rong, C. Wang, L. Chen, Y. Yan and Y. Cheng, *Sci. Adv.*, 2020, **6**(33), eaaz1774.
20 E. Klein, M. Ciobanu, J. Klein, V. MacHi, C. Leborgne, T. Vandamme, B. Frisch, F. Pons, A. Kichler, G. Zuber and L. Lebeau, *Bioconjugate Chem.*, 2010, **21**(2), 360–371.
21 J. Gaucheron, C. Santaella and P. Vierling, *Bioconjugate Chem.*, 2001, **12**(1), 114–128.
22 J. Xu, J. Lv, Q. Zhuang, Z. Yang, Z. Cao, L. Xu, P. Pei, C. Wang, H. Wu, Z. Dong, Y. Chao, C. Wang, K. Yang, R. Peng, Y. Cheng and Z. Liu, *Nat. Nanotechnol.*, 2020, **15**(12), 1043–1052.
23 J. Gaucheron, C. Santaella and P. Vierling, *Biochim. Biophys. Acta, Biomembr.*, 2002, **1564**(2), 349–358.
24 H. Saito, W. Shinoda and M. Mikami, *J. Phys. Chem. B*, 2008, **112**(36), 11305–11309.
25 M. J. Landsberg, J. L. Ruggles, W. M. Hussein, R. P. McGeary, I. R. Gentle and B. Hankamer, *Langmuir*, 2010, **26**(24), 18868–18873.
26 M. C. Gagnon, M. Auger and J. F. Paquin, *Org. Biomol. Chem.*, 2018, **16**(27), 4925–4941.
27 Z. Zhang, W. Shen, J. Ling, Y. Yan, J. Hu and Y. Cheng, *Nat. Commun.*, 2018, **9**, 1377.
28 J. Gaucheron, C. Santaella and P. Vierling, *J. Gene Med.*, 2001, **3**(4), 338–344.
29 M. S. Fernandez and P. Fromherz, *J. Phys. Chem.*, 1977, **81**(18), 1755–1761.
30 L. Miao, J. Lin, Y. Huang, L. Li, D. Delcassian, Y. Ge, Y. Shi and D. G. Anderson, *Nat. Commun.*, 2020, **11**, 2424.
31 M. Jayaraman, S. M. Ansell, B. L. Mui, Y. K. Tam, J. Chen, X. Du, D. Butler, L. Eltepu, S. Matsuda, J. K. Nara-yanannair, K. G. Rajeev, I. M. Hafez, A. Akinc, M. A. Maier, M. A. Tracy, P. R. Cullis, T. D. Madden, M. Manoharan and M. J. Hope, *Angew. Chem., Int. Ed.*, 2012, **51**(34), 8529–8533.
32 M. A. Maier, M. Jayaraman, S. Matsuda, J. Liu, S. Barros, W. Querbes, Y. K. Tam, S. M. Ansell, V. Kumar, J. Qin, X. Zhang, Q. Wang, S. Panesar, R. Hutabarat, M. Carioto, J. Hettinger, P. Kandasamy, D. Butler, K. G. Rajeev, B. Pang, K. Charisse, K. Fitzgerald, B. L. Mui, X. Du, P. Cullis,

T. D. Madden, M. J. Hope, M. Ma-noharan and A. Akinc, *Mol. Ther.*, 2013, **21**(8), 1570–1578.
33 M. Schlich, R. Palomba, G. Costabile, S. Mizrahy, M. Pannuzzo, D. Peer and P. Decuzzi, *Bioeng. Transl. Med.*, 2021, **6**(2), 1–16.
34 P. Paramasivam, C. Franke, M. Stöter, A. Höijer, S. Bartesaghi, A. Sabirsh, L. Lindfors, M. Yanez Arteta, A. Dahlén, A. Bak, S. Andersson, Y. Kalaidzidis, M. Bickle and M. Zerial, *J. Cell Biol.*, 2022, **221**(2), 1–20.
35 L. Miao, Y. Zhang and L. Huang, *Mol. Cancer*, 2021, **20**(1), 1–23.